PAPER • **OPEN ACCESS**

Dual lidar wind measurements along an upstream horizontal line perpendicular to a suspension bridge

To cite this article: M Nafisifard *et al* 2021 *IOP Conf. Ser.: Mater. Sci. Eng.* **1201** 012008

Dual lidar wind measurements along an upstream horizontal line perpendicular to a suspension bridge

M Nafisifard[1,*], J B Jakobsen[1], E Cheynet[2], J T Snæbjörnsson[1,3], M Sjöholm[4] and T Mikkelsen[4]

[1]Department of Mechanical and Structural Engineering and Material Science, University of Stavanger, Kjell Arholmsgate 41, Stavanger, Norway.
[2]Bergen Offshore Wind Centre and Geophysical Institute, University of Bergen, Bergen, Norway.
[3]Department of Engineering, Reykjavik University, Menntavegur 1 IS-101, Reykjavík, Iceland.
[4]Department of Wind Energy, Technical University of Denmark, Frederiksborgvej 399, 4000 Roskilde, Denmark.

E-mail: *mohammad.nafisifard@uis.no

Abstract. Remote wind sensing can complement traditional anemometry at a bridge site and contribute to an improved wind-resistant design of long-span bridges. This study examines wind lidar measurement data recorded along a 168-meter-long horizontal line perpendicular to the main span of a suspension bridge in complex terrain. The velocity data records are obtained by a pair of continuous-wave Doppler lidars (short-range WindScanners) installed on the bridge deck. The measurement data are explored in terms of the mean wind speed and mean wind direction upstream of the bridge. The spectral characteristics of turbulence along the line are also investigated in relation to the increasing sampling volumes of a continuous-wave lidar system at increasing distances from the monitored area. Wind characteristics observed by the lidars are compared to those derived from sonic anemometer data recorded above the bridge deck at midspan. The results provide new insight into the wind flow characteristics in a fjord and demonstrate the potential of lidar measurements in charting the wind flow around a bridge. A slight monotonic increase of the wind speed, as well as a decrease in the yaw angle, is observed as the distance to the bridge reduces from 160 m to 20 m, while lower wind velocities are accompanied by a more stable wind direction. Within 15 m from the bridge deck, the adopted lidar setup gives unreliable information due to the large angle between the lidar beams.

1. Introduction

Wind velocity is traditionally measured using anemometers that need to be installed at a single point of interest, usually utilizing a mast or a tower. For fjord crossings, tower installations are only possible on land on either side of the fjords. Generally such monitoring positions give limited information on the wind conditions in the middle of the fjord, and thereby the loading on the bridge structure crossing the fjord [1].

In the recent decade, optical remote wind sensing instruments, such as Doppler wind lidars, have been developing rapidly. They make it possible to assess the wind conditions in the middle of the fjords to improve the loading information required for bridge design [2]. Lidars can complement the traditional tower-based anemometry and provide valuable data on local wind conditions in inaccessible regions leading to a safer design of structural elements such as piers and the deck of long-span bridges. Flow mapping along the planned crossing, above the water surface, can be performed by long-range, pulsed Doppler lidars installed onshore, with a measurement reach of several kilometres.

Continuous-wave Doppler wind lidars, with smaller sampling volumes at shorter measurement distances than pulsed Doppler lidars, introduce a complementary capability to observe wind flow around an existing structure in greater details [2], while the recorded data are not influenced by masts, which may distort the flow [3]. This study makes use of data from two synchronized continuous-wave short-range Doppler lidars (WindScanners) that were deployed on an existing suspension bridge crossing the inlet of a fjord to investigate the wind field in the vicinity of the deck.

In a previous study, the same lidar system was used to evaluate the coherence of the along-wind and across-wind velocity components along a line parallel to the deck [4]. The research showed good agreement between lidars and sonic anemometers measurements above the bridge deck for the mean and standard deviation of the horizontal wind velocity. The length scale estimated based on lidar data was up to 29% higher than the one evaluated from the sonic anemometer data. In the same measurement campaign, flow conditions along a vertical line at a distance of three deck widths from the bridge were also studied [5]. The velocity deficit observed by the lidars in the bridge wake allowed the estimation of the drag coefficient. The latter was found to be consistent with the design value evaluated in wind tunnel studies [6]. Also, a broad-banded vortex shedding was observed for frequencies above 0.1 Hz.

This paper extends the studies done in [4, 5] by utilizing additional lidar data from the campaign in May 2014 to explore turbulence along a horizontal line perpendicular to the bridge deck. The incoming turbulent flow was monitored at distances up to 13B (160 m) upstream of the bridge's deck, where B is the width of the deck ($B = 12.3$ m). As the flow measurements close to the girder are valuable in relation to the bridge deck aerodynamics, the reliability of the lidar data close to the deck is discussed hereinafter.

The paper is organized as follows: Section 2 describes the measurement site and provides basic information on the Lysefjord bridge and its instrumentation. Section 3 discusses the lidar measurement setup and the methods used when evaluating the wind data and the single-point wind statistics. Section 4 documents the change of the mean wind speed, yaw angle, and velocity spectrum as a function of the distance from the deck. Finally, the measurement uncertainties are discussed using the condition number and some guidelines are provided for further works.

2. Measurement site and monitoring system

The Lysefjord bridge is a suspension bridge constructed in 1997 at the inlet of a narrow and deep fjord with a main span of 446 m (fig. 1). The bridge's elevation at midspan is 55 m above sea level, and the bridge stretches from North-West to South-East. The two dominant wind directions are from the North-Northeast (outwards the fjord) and the South-Southwest (inwards the fjord). The flow from these two sectors has notably different turbulent characteristics.

The WindScanner system comprised of two synchronized continuous-wave wind lidars was installed on the Lysefjord suspension bridge (fig. 1 and fig. 2). The technical properties of the lidars are presented in Table 1. Both lidars had a 3-inch-wide optical telescope and a rotating double-prism head allowing for scanning within a cone with a half opening angle of 60°. The two lidars, namely R2D1 and R2D3, were located on the west side around the center of the bridge deck about 90 m apart. The distance between the two lidars was adopted following the main target of the campaign, which was to characterise the undisturbed wind flow southwest of the bridge.

This study utilizes data from a sonic anemometer installed on hanger 18 at the center of the bridge span, about 6 m above the deck, (fig. 2). The sonic anemometer was a WindMaster Pro 3-Axis Anemometer from Gill Instrument and operated with a sampling frequency of 32 Hz. It is used as a reference sensor since it is located between the two lidars, on the upwind side of the deck. In addition, a Vaisala weather transmitter provided the temperature during the measurement period, which was stable, fluctuating between 21.4 °C and 21.7 °C.

Figure 3 illustrates the measurement setup with two wind lidars, jointly overlooking the horizontal line perpendicular to the bridge axis, at the bridge mid-span. The coordinate system for the wind components is shown in fig. 3. The lidars record the velocity along the line-of-sight in a "thin" bell-shaped volume centered at the focus distance. The thick blue X-markups in fig. 3 indicate the size of the sampling

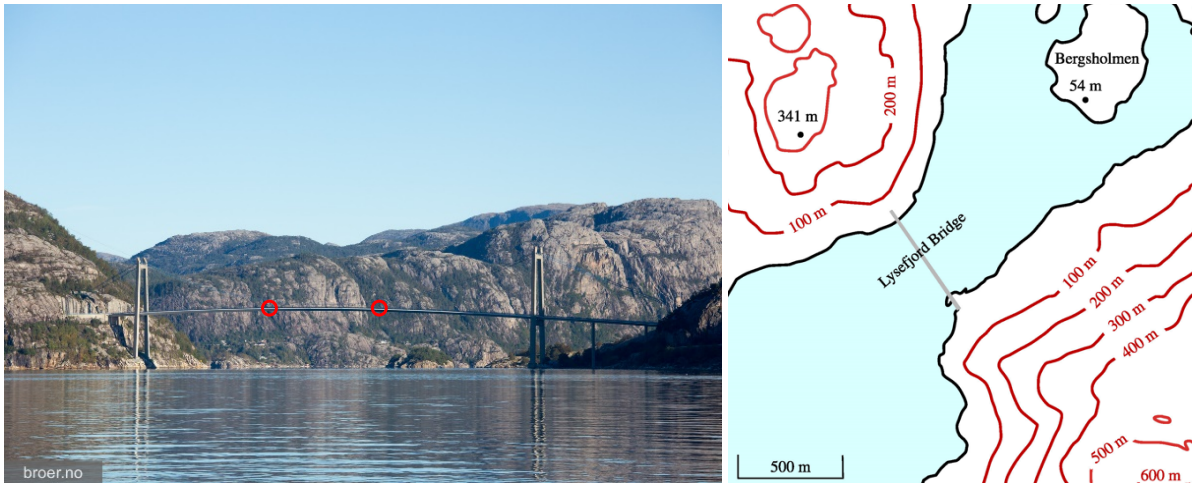

Figure 1. The Lysefjord Bridge (left) view from the West, with location of the lidars on the West side of the bridge denoted by circles and (right) its position on the map (from [5]).

Figure 2. Wind sensors on the Lysefjord Bridge: (left) Short-range WindScanner [5] and (right) WindMaster Pro 3D sonic anemometer at midspan.

volumes, at selected distances, in terms of the so-called full width at half maximum (FWHM) (see section 3.2). The measurements are performed in a horizontal plane 1.4 m above the bridge deck located 55 m above the sea surface. The angles between the beams and the bridge deck axis for the lidars R2D1 and R2D3 are denoted α_1 and α_2, respectively.

Both lidars aim at the same point along the scanning line starting at 0.5 m and ending 168 m from the deck. A full measurement cycle forth and back along the scanning line lasts for 1 second and contains 390 measurement points. The scanning sequence, in both directions along the line, results in an almost triangular waveform as a spatiotemporal pattern for the intersection of two scanning beams.

3. Analysis methods

Because of the specific scanning pattern, the sampling frequency at each specific distance varies along the scanning line except for the middle and two endpoints, which necessitates a resampling of the data by

Table 1. Properties of the Doppler wind lidar short-range WindScanner system [4, 5] installation.

Properties	Values
Wavelength	1.565 μm
Shortest range	approx. 10 m
Longest range	approx. 200 m
Scan line sweep frequency	1 Hz
Scan line sweep length	168 m
Line-of-sight (LOS) sampling frequency	390 Hz
Lidars LOS detection range	-21 $\mathrm{m\,s^{-1}}$ to +18 $\mathrm{m\,s^{-1}}$

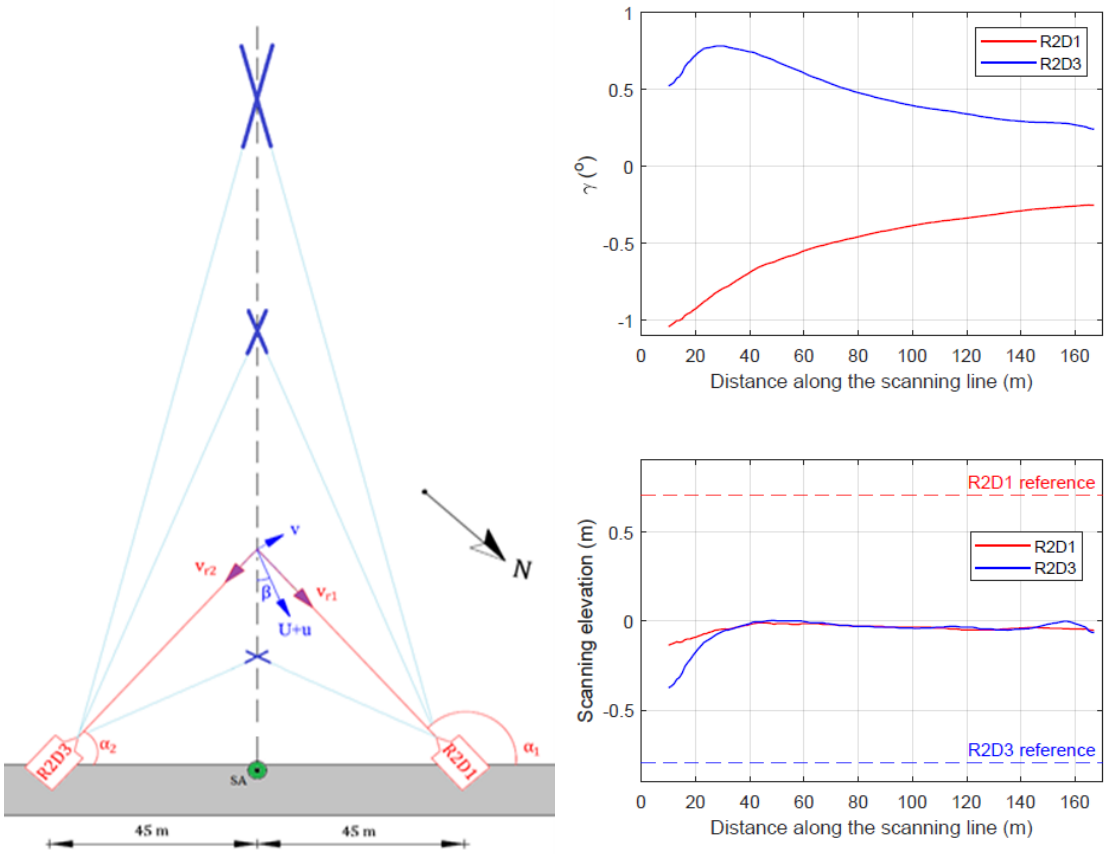

Figure 3. (left) Plan view of the measurement setup, (right-top) variation of line-of-sight beams' angles from the horizontal plane γ with respect to the horizontal plane of measurement, (right-bottom) elevation difference between lidars and measurement points.

linear interpolation with a uniform sampling frequency of 1 Hz leading to a Nyquist frequency of 0.5 Hz, accordingly.

Since two lidars were used, the scanning beams were located within the scanned plane of interest in order to avoid the influence from the third wind component perpendicular to that plane. This scanning principle combined with the curvature of the bridge axis in the vertical plane leads to a tilt of the scanning axis along the bridge of 0.95°. As part of the initial data analysis, it is useful to investigate to what degree this tilt angle influences the results. Figure 3 shows the tilt angle γ encountered along the horizontal

scanning line, which reduces as the distance from the bridge deck increases. In addition to the vertical beam related to the bridge axis curvature, a secondary contribution to the results in fig. 3 comes from limited variations in the attained scanning heights along the observation line. The height variations are displayed in fig. 3, with the vertical axis magnified about 100 times with respect to the horizontal one, for enhanced visibility. The largest resulting tilt angles, which are encountered close to the bridge deck, correspond to a contribution of the vertical turbulence component smaller than 2% in the line-of-sight velocity records of the nominally horizontal wind speed. The contribution consequently becomes even smaller as the distance from the bridge deck increases.

3.1. Wind velocity formulation

By using the along-beam wind velocity data from two synchronized lidars in a horizontal plane tangential to the vertically curved bridge (v_{r_1} and v_{r_2}), it is possible to extract the wind components in any arbitrary direction in the horizontal plane (see fig. 3), provided that the scanning beams intersects with angles as close as possible to 90°. The components perpendicular and along the bridge deck (v_x and v_y) as well as the along-wind and across-wind components (u and v) are determined using the following mathematical transformations [7]:

$$\begin{bmatrix} v_x \\ v_y \end{bmatrix} = \mathbf{M}^{-1} \begin{bmatrix} v_{r_1} \\ v_{r_2} \end{bmatrix} \tag{1}$$

where

$$\mathbf{M} = \begin{bmatrix} \sin(\alpha_1) & -\cos(\alpha_1) \\ \sin(\alpha_2) & -\cos(\alpha_2) \end{bmatrix}. \tag{2}$$

In equation (1), the inverse of matrix $\mathbf{M}$ is required to solve a system of linear equations and obtain the velocity components perpendicular and along the bridge deck. The sensitivity of the evaluation of the velocity components in equation (1) to the changes in the transformation matrix shown in equation (2) can partly be revealed by the condition number of the matrix. Higher condition number, indicates larger uncertainty in the obtained wind velocity components. If the equation system is ill-conditioned, the condition number is considerably greater than unity and the retrieval algorithm can give unreliable results.

To compute u and v, the following transformation is used:

$$\begin{bmatrix} u \\ v \end{bmatrix} = \begin{bmatrix} \cos(\beta) & \sin(\beta) \\ -\sin(\beta) & \cos(\beta) \end{bmatrix} \begin{bmatrix} v_x \\ v_y \end{bmatrix} \tag{3}$$

where β is the yaw angle defined as

$$\beta = \arctan\left(\frac{\overline{v}_y}{\overline{v}_x}\right). \tag{4}$$

In the above equation, $\overline{v}_x$ and $\overline{v}_y$ are the time-averaged values of the velocity components along and across the deck, respectively, within each distinct interval associated with a specific target distance from the bridge deck. The instantaneous horizontal wind data along the lidar scanning beam, can be processed to retrieve the associated along-wind and across-wind velocity components, denoted by u and v, respectively. The along- and across wind components are decomposed into a mean part and a fluctuating part with zero mean, as follows

$$u = \overline{u} + u' \tag{5}$$

$$v = \overline{v} + v' \tag{6}$$

where $\overline{v}$ is approximatively $0\ \mathrm{m\,s^{-1}}$.

Based on the instantaneous wind velocity time series, the power spectral densities are calculated using the Welch method [8]. Records are divided into three segments with 50% overlapping [9]. Then, the spectral data are bin-averaged using a logarithmic-spaced frequency interval.

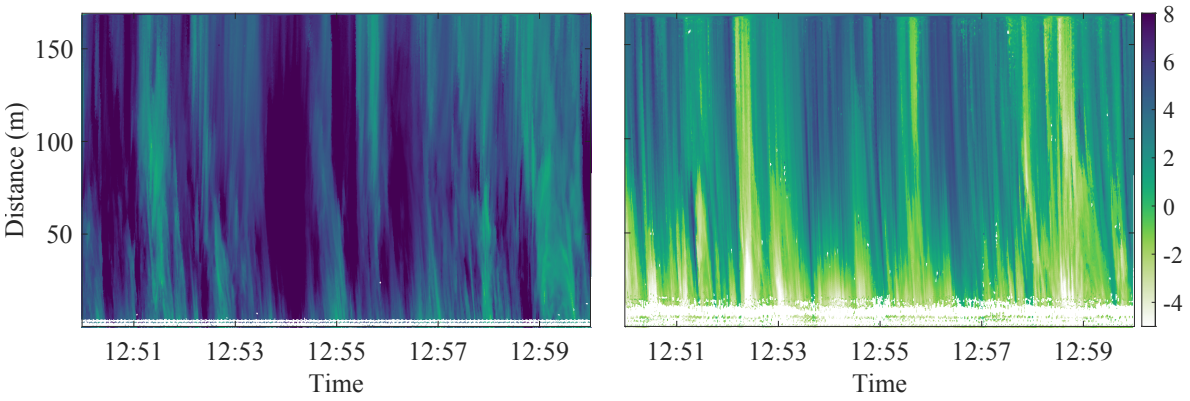

Figure 4. Spatiotemporal fluctuations of wind velocity recorded on 22 May 2014, 12:50 to 13:00 by the two lidar instruments (left) R2D1 and (right) R2D3.

3.2. The lidar data resolution

The full width at half maximum (FWHM) expresses the spatial resolution of a continuous-wave lidar [10] and is proportional to the square of the distance between the lidar and the focus "point",

$$\mathrm{FWHM} = \frac{\lambda r^2}{\pi a_0^2} \tag{7}$$

where $\lambda = 1.565\ \mu\mathrm{m}$ is the wavelength of the laser source; r is the scanning distance and $a_0 \approx 20$ mm is the effective beam radius.

In the present study, the FWHM fluctuates between 2.5 m and 38 m, which corresponds to scanning distances from 45 m up to ca. 174 m.

3.3. Normalized Doppler spectrum maxima

To quantify the lidar data quality, the Normalized Doppler Spectrum Maximum (NDSM) [5] is used in this study to select the data with high intensity of the back-scattered signal. The NDSM is the ratio between the maximum of the Doppler spectrum and the mean background noise spectrum. An NDSM value of 1.17 was arbitrarily considered here, as in [5], as the minimum acceptable value for all data points. The lidar readings associated with the NDSM under 1.17 or line-of-sight velocity equal to zero were considered unreliable and disregarded.

4. Results

4.1. Wind velocities based on WindScanner data

The spatial and temporal resolution of the deployed WindScanner system is suitable to study the horizontal wind velocity field up to two hundred meters from the instruments. Figure 4 shows the line-of-sight velocities recorded by the two lidars, R2D1 and R2D3, as a function of distance from the bridge and time, during a selected 10-minute interval.

While the R2D1 unit captures the velocity components from 1 $\mathrm{m\,s^{-1}}$ to 10 $\mathrm{m\,s^{-1}}$ along the scanning line, the R2D3 lidar records the values between -4 $\mathrm{m\,s^{-1}}$ and 5 $\mathrm{m\,s^{-1}}$. The R2D1 lidar beams are thus more aligned with the incoming flow than the R2D3 unit, which observes the lower wind velocities, with a changing sign along the scanning line. Close to the bridge, the R2D3 lidar is also seen to have more data with high background noise in the lidar spectra as described in section 3.3 or zero line-of-sight velocities. This type of data is shown in fig. 4 as white points close to the bridge deck. As illustrated in fig. 5, the fraction of the measurement data with sufficiently low background noise in the lidar spectra for this unit

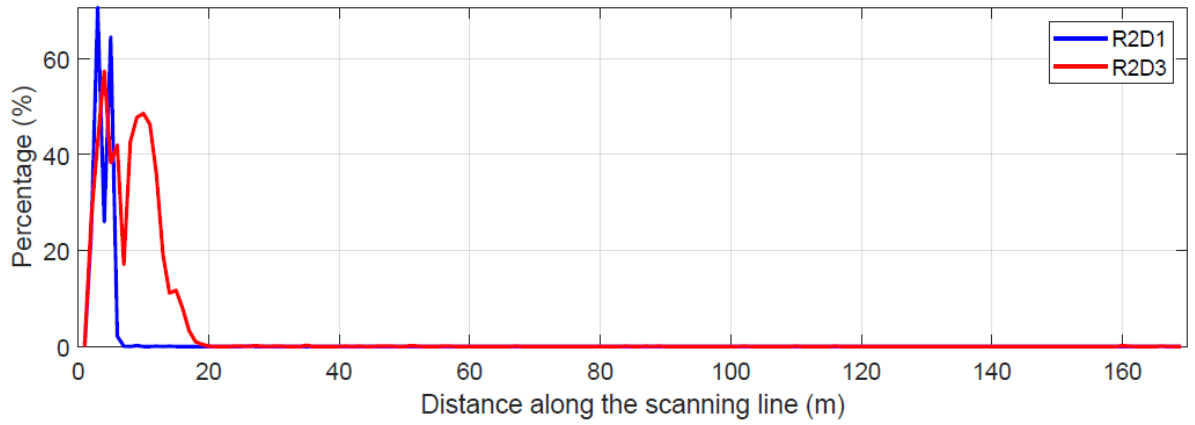

Figure 5. Relative number of unreliable data points as a function of the distance from the bridge, for the recordings shown in fig. 4.

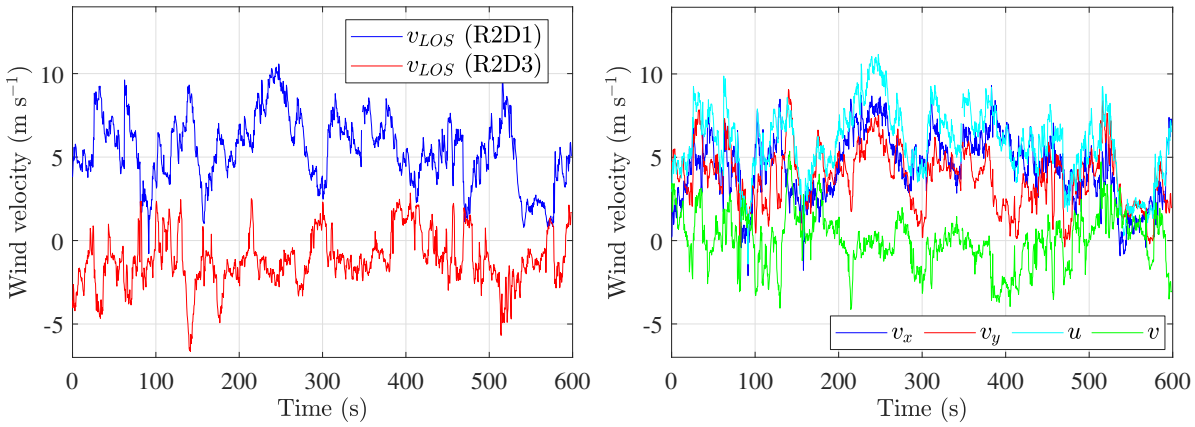

Figure 6. (left) Line-of-sight velocity components measured by WindScanners 25 meters from the deck on 22 May 2014, 12:50 to 13:00. (right) Time-series of the along-wind (u) and across-wind velocity components (v) 25 m in front of the deck, as well as the components along- (v_x) and normal to the bridge deck (v_y), recorded on 22 May 2014, from 12:50 to 13:00.

decreases to below 50% at distances smaller than 10 m. The R2D1 lidar records also include noisy data closer to the bridge deck, for distances smaller than 5 m.

In fig. 6 (panel to the left), variations of the line-of-sight velocities of both lidars are shown. At the selected distance of 25 meters from the deck, it can be observed that the two line-of-sight velocities have opposite variations, which is also visible in fig. 4, since the angle between both beams is relatively wide, or around 120°. The right panel of fig. 6 shows the same data expressed in terms of the wind velocity components in the along- and crosswind direction, as well as the components along and normal to the bridge axis.

4.2. Comparison of the sonic anemometer and lidar observations

Figure 7 displays the 10-min mean wind speed and mean wind direction, along the scanning line, based on the data recorded on 2014-05-22.

All 10-minute intervals with mean wind velocities higher than 5.5 $\mathrm{m\,s^{-1}}$ show a slight monotonic increase of the mean wind speed closer to the deck and a reduction of the mean yaw angle. On the other

hand, the 10-minute periods with mean wind velocities lower than 4.5 $\mathrm{m\,s^{-1}}$ on average, show a more stable yaw angle along the scanning line. The mean wind speed increase towards the bridge deck is likely due to a narrowing of the fjord inlet at the studied location.

The first interval, from 12:30 to 12:40, which has the highest yaw angle (approximately 50°) compared to others, is clearly influenced by the geometry of the fjord as the wind speed increases from 3.5 $\mathrm{m\,s^{-1}}$ at the largest scanning distance to 5 $\mathrm{m\,s^{-1}}$ at the deck position.

Between 12:50 and 13:00, an increase in the mean wind speed, from about 5.8 $\mathrm{m\,s^{-1}}$ at x= 150 m to 6.2 $\mathrm{m\,s^{-1}}$ at x= 80 m can be identified and associated with a minor decrease in the yaw angle of $\beta = 45°$, corresponding to 185° with respect to north. For distances smaller than x= 80 m, a reduction in mean wind speed to about 5.8 $\mathrm{m\,s^{-1}}$ at x= 25 m is observed, as well as an additional reorientation of the flow to a yaw angle of 40°.

Within two bridge deck widths upstream of the bridge, a significant increase in the mean wind speed is observed. Wind characteristics observed close to the deck indicate a velocity speed-up 1.4 m above the deck surface, as the flow adapts to the bridge obstacle, associated with a reduction of the yaw angle. While such observations qualitatively seem plausible, they are associated with large uncertainties, due to the large angle between the lidar beams, which exceeds 150°, for distances from the deck smaller than 10 m. Since the R2D3 lidar recordings include noisy line-of-sight wind data close to the bridge (see fig. 4 and fig. 5), scanning regions with high uncertainty are extended to 15 m upstream of the deck, as marked by the red zone in fig. 7.

In Fig 8, the markers at a scanning distance of zero meter represent the data recorded by the sonic anemometer 6 m above the deck. They agree well with the wind conditions mapped by the lidars approximately 20 m to 25 m from the deck. The result serves as an additional validation of the lidar measurement methodology in the given site conditions. It also indicates that the sonic anemometer measurements of the upstream flow, taken 6 m above the deck at the location of hangers and main cables, can be considered free of the disturbances from the bridge deck.

Between 12:50 and 13:00, the sonic anemometer recorded a turbulence intensity for the along-wind component equal to 0.33. The same value was found by the lidars data considering scanning distances 20 m and 120 m.

Figure 8 presents the power spectral density (PSD) estimates of the along-wind and cross-wind velocity components, computed using the lidar and anemometer data and expressed as a function of the wave number as follows.

$$k_1 = \frac{2\pi f}{\overline{u}}. \tag{8}$$

For the WindScanner data, distances at 25, 50, and 100 m away from the deck were selected. While the spectral contents derived from the lidar measurements and the sonic data are in overall agreement, an attenuation of turbulence components for wave numbers above $0.1\,\mathrm{m^{-1}}$ by the WindScanners is visible, in addition to some spectral peaks around the Nyquist frequency. The attenuation observed is due to the low-pass filtering effect caused by the sampling volume averaging of the lidars [11]. No clear difference is visible between the turbulent spectra at a scanning distance of 25 m, 50 m, and 100 m, which suggests that the narrowing of the fjord does not significantly affect the spectral characteristics of the two horizontal wind components in the vicinity of the bridge.

4.3. Error propagation in the retrieved lidar data

Figure 9 shows the variation of the condition number with the distance from the bridge deck. Close to the bridge deck, where the angle between the lidar beams increases, the condition number raises. A condition number of 5 and 10 correspond to a distance of 8 m and ca. 4 m, respectively. Consequently, wind characteristics calculated within the first 10-meter distance from the bridge deck are not considered reliable. At this distance, the angle between lidar beams corresponds to 150° or more, and the hangers may interfere with the lidar beams. As discussed earlier, the low quality data recorded by the R2D3 close to the bridge, extend the unreliable data range to 15 m in front of the deck.

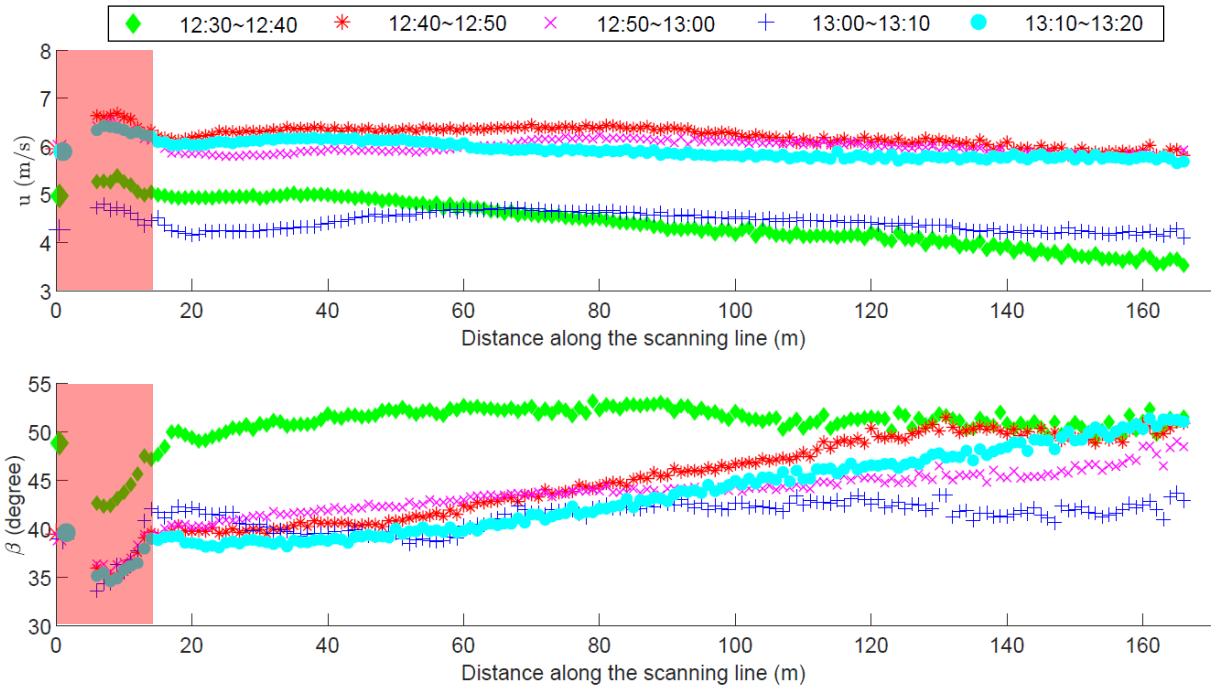

Figure 7. (Top) Mean wind speed and (Bottom) mean yaw angle recorded by WindScanners and the sonic anemometer at midspan on 22.5.2014. The red shaded areas indicate scanning distances with large measurement uncertainties.

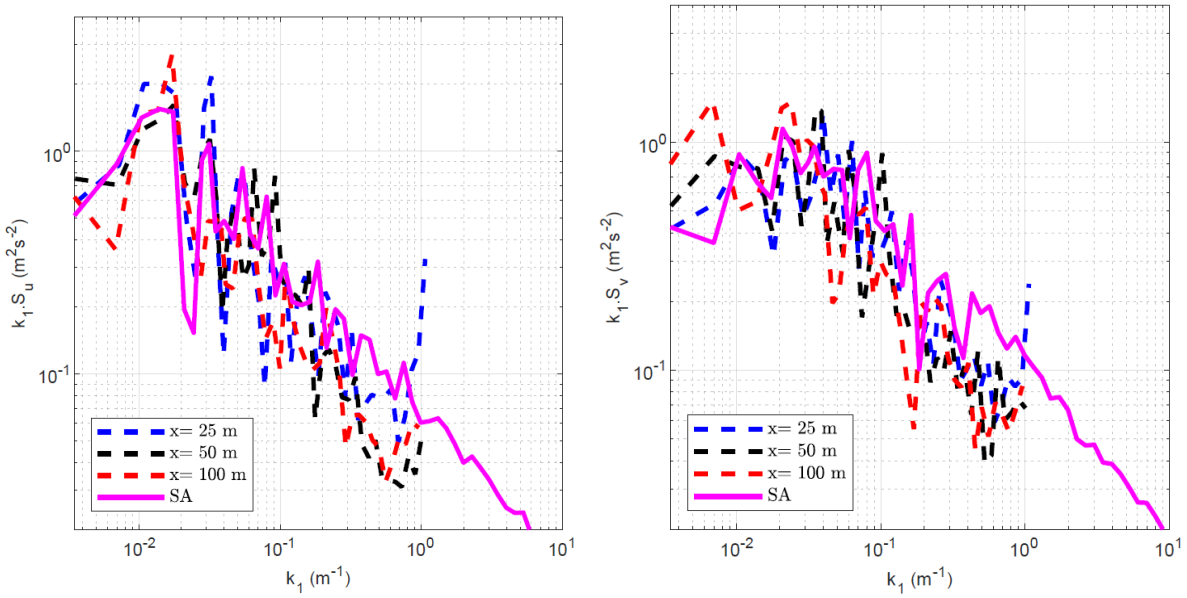

Figure 8. (left) Power spectral density estimates of the along-wind. (right) the cross-wind velocity component computed using the WindScanners sonic anemometer data on 2014-05-22 from 12:50 to 13:00.

5. Conclusions and further works

Two Doppler lidars (short-range WindScanners) were deployed on the Lysefjord bridge in 2014 to study the wind flow in a complex fjord terrain in Norway. The lidars focused along a horizontal line

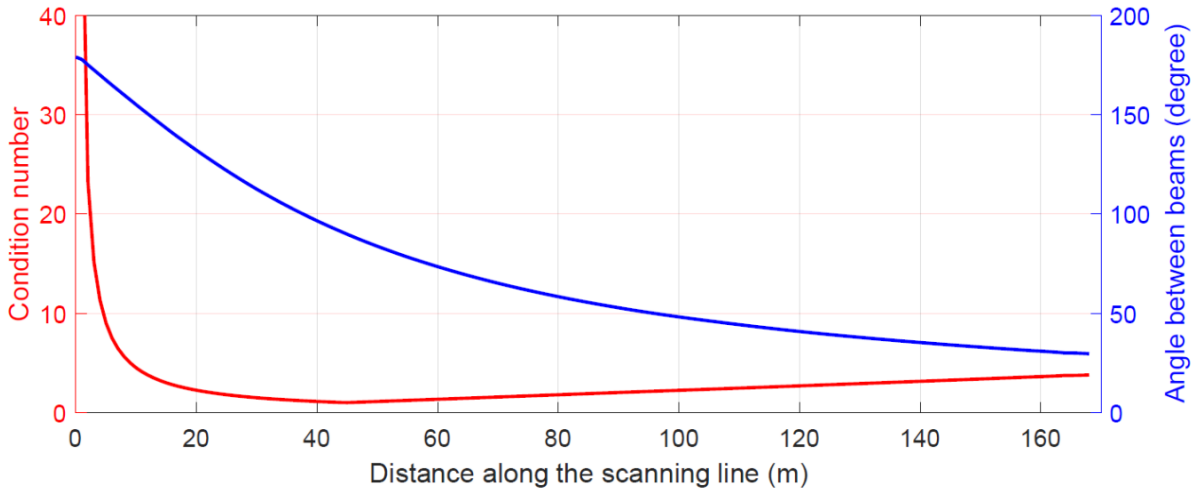

Figure 9. Condition number and angle between the scanning beams as a function of distance from the bridge.

perpendicular to the bridge axis to study the turbulent flow upstream of the deck. The measurement data are explored in terms of the mean wind velocity, mean wind direction as well as the one-point power spectral densities at multiple distances along the scanning line. The main findings of this study are as follows:

- The lidar instruments document a slight increase of the mean wind speed and a slight decrease of the yaw angle as the flow moves toward the bridge, reflecting the local influence of the narrowing of the fjord inlet on the mean flow characteristics. Results further show that lower wind velocities are accompanied by a more stable variation of wind directions along the scanning line.
- Within 20 m distance from the bridge deck, corresponding to 1.6 bridge deck widths, a notable mean wind speed increase is observed together with a reduction of the wind yaw angle. However, such an observation is associated with large uncertainties close to the bridge deck, in particular for distances below 15 m. This is partly due to the low projected wind speed on the line-of-sight of one of the two lidars and partly due to the large angles between the lidar beams close to the deck.
- A good agreement was found between the mean wind velocities and wind direction measured with the lidars and the sonic anemometer at about 25 m from the deck.
- The spectral contents derived from the lidar measurements, and the sonic data are in overall agreement. The velocity spectra at 25 m, 50 m, and 100 m were similar, suggesting no significant variation of the spectral characteristics of turbulence due to e.g. the narrowing of the fjord inlet.

The configuration of the short-range WindScanner lidar system used in this study allowed the extraction of wind characteristics by scanning in a nearly horizontal plane, allowing the retrieval of two velocity components of the flow. To get the third velocity component a different configuration must be used. For instance, a system of three synchronized CW wind lidars can record 3D wind and turbulence data, and those data could then be analysed to evaluate both first and second-order wind statistics for the three turbulence components. In addition, a smaller distance between the lidars in a dedicated measurement setup would facilitate observations of the wind-deck interaction in greater detail. Such an experiment has been ongoing at the Lysefjord bridge between August 2021 and October 2021.

Acknowledgments
The presented data analysis is performed as part of the H2020-MSCA-ITN-2019 project funded by the European Union, grant number 858358. The authors acknowledge the support of the Norwegian Public Roads Administration in carrying out the lidar measurement campaign.

References
[1] Midjiyawa Z, Cheynet E, Reuder J, Ágústsson H and Kvamsdal T 2021 *J. Wind Eng. Ind. Aerodyn.* **211** 104584
[2] Mikkelsen T, Sjöholm M, Angelou N and Mann J 2017 *IOP Conf. Ser.: Mater. Sci. Eng.* vol 276 (IOP Publishing) p 012004
[3] Cheynet E, Jakobsen J B and Snæbjörnsson J 2019 *J. Sound Vib.* **450** 214–230
[4] Cheynet E, Jakobsen J B, Snæbjörnsson J, Mikkelsen T, Sjöholm M, Mann J, Hansen P, Angelou N and Svardal B 2016 *Exp. Fluids* **57** 1–17
[5] Cheynet E, Jakobsen J B, Snæbjörnsson J, Angelou N, Mikkelsen T, Sjöholm M and Svardal B 2017 *J. Wind Eng. Ind. Aerodyn.* **171** 261–272
[6] Hjorth-Hansen E 1987 Askøy Bridge: Wind Tunnel Tests of Time-average Wind Loads for Box-girder Bridge Deck Tech. rep. SINTEF report STF71 A87037 SINTEF.
[7] Newsom R, Calhoun R, Ligon D and Allwine J 2008 *Boundary Layer Meteorol.* **127** 111–130
[8] Welch P 1967 *IEEE Trans. Audio Electroacoust.* **15** 70–73
[9] Carter G, Knapp C and Nuttall A 1973 *IEEE Trans. Audio Electroacoust.* **21** 337–344
[10] Mikkelsen T 2009 *European Wind Energy Conference and Exhibition* vol 6 pp 4123–4132
[11] Angelou N, Mann J, Sjöholm M and Courtney M 2012 *Rev. Sci. Instrum.* **83** 033111